Original scientific paper

DYNAMIC ANALYSIS OF THE RIGID-FLEXIBLE EXCAVATOR MECHANISM BASED ON VIRTUAL PROTOTYPE

Yongliang Yuan[1], Jianji Ren[2], Zhenxi Wang[2], Xiaokai Mu[3]

[1]School of Mechanical and Power Engineering, Henan Polytechnic University, Jiaozuo, China
[2]School of Computer Science and Technology, Henan Polytechnic University, Jiaozuo, China
[3]School of Mechanical Engineering, Dalian University of Technology, Dalian, China

Abstract. *In this paper, the excavator's dynamic performance is considered together with the study of its trajectory, stress distribution and vibration. Many researchers have focused their study on the kinematics principle while a few others focused their work on dynamic performance, especially the vibration analysis. Previous studies of dynamic performance analysis have ignored the vibration effects. To address these challenges, the rigid-flexible coupling model of the excavator attachment is established and carried out based on virtual prototyping in this study. The dipper handle, the boom and the hoist rope are modeled as a flexible multi-body system for structural strength. The other components are modeled as a rigid multi-body system to catch the dynamic characteristics. The results show that the number of flexible bodies has little effect on the excavation trajectory. The maximum stress determined for the dipper handle and the boom are 96.45 MPa and 212.24 MPa, respectively. The dynamic performance of the excavator is greatly influenced by the clearance and is characterized by two phases: as the clearance decreases, the dynamic response decreases at first and then increases.*

Key Words: *Excavator, Dynamics, Virtual Prototype, Rigid-flexible Coupling*

1. INTRODUCTION

Excavators are widely used as primary production equipment for surface mining operations. In practical engineering, the dynamic response of an excavator reflects its performance. The conventional design process uses a laboratory test to simulate the physical prototype in order to evaluate the excavator performance, which is very costly and time-consuming for investigating the dynamic performance of the physical prototype [1].

Recently, virtual prototype simulators have been widely used to simulate surface mining equipment [2]. In order to improve the dynamic performance of the excavator, it is necessary to build the excavator model based on the virtual prototype technology just as to build a physical prototype. For this purpose, the excavator could be analyzed based on a dynamics model. Many kinematic and dynamics models of excavators were studied in the last decades [3,4], For example, Li et al. [5] conducted an excavator model study and confirmed its feasibility with the virtual prototype software; they obtained its kinematics principle. Frimpon et al. [6] used Newton-Euler to establish the dynamics model and obtained the displacement, the speed and the acceleration of an excavator in ADAMS. Šalinić et al. [7] established the Lagrange equation model to obtain the kinematics principle of the excavator. Awuah-Offei et al. [8] proposed the numerical method and obtained the lifting speed and thickness of cutting relational curves. Mitrev et al. [9] developed a plane multi-body mechanical model of a hydraulic excavator, and proved its applicability. Ding et al. [10] proposed a new dynamic mathematical model, which broadened the scope of excavation and improved the excavating force. Though the kinematics principle of excavators has been well studied, most of the previous work only dealt with a rigid multi-body system of the excavator rather than a more realistic rigid-flexible system.

The excavator is a typical rigid-flexible coupling system, which could influence the dynamic performance. However, there are a few studies on the rigid-flexible coupling of excavators. Ma used Matlab/Simulink to establish the model and carry out the simulation [11]. He et al. [12] used the rigid rod to replace the steel wire rope to establish the virtual prototype model, and carried out the simulation. He et al. [13] established the flexible body of the rope and obtained the stress change trend of the wire during the digging stage. Jiang et al. [14] established the rigid-flexible coupling model of hydraulic excavators and obtained the vibration performance. Strzalka et al. [15,16] offered an approach to *a priori* estimation with areas of the structure exposed to high stresses, which is decisive for a highly efficient fatigue analysis. Zhao et al. [17] established a rigid-flexible coupling model, and obtained the stress of the key points in the cracked area. The above researchers focused on stress of the components based on the rigid-flexible coupling model and have not yet conducted a vibration analysis, especially the effect of the assembly clearance on the vibration of the excavator attachment.

In order to investigate the dynamic performance of excavator attachments, this paper proposes a rigid-flexible coupling model based on virtual prototyping. The reminder of the paper is organized as follows: Section 2 contains the structural components of the excavator and kinematic sketch of attachment. Establishment of rigid-flexible coupling model is described in Section 3. Section 4 presents the numerical simulation settings. Section 5 discusses the simulation results, especially the effect of different clearances on the boom and the dipper handle. Section 6 gives the concluding remarks and future work.

2. THE STRUCTURAL COMPONENTS OF THE EXCAVATOR AND KINEMATIC ANALYSIS

2.1. Structural Components of the Excavator

The excavator is complex major equipment, which is mainly utilized in construction, mining, etc. The excavator has many advantages, including simple operation, low strength of the workers and high efficiency. The excavator consists of three major components, including the upper body, the lower body and the attachment. The whole system and main components of the excavator are shown in Fig. 1.
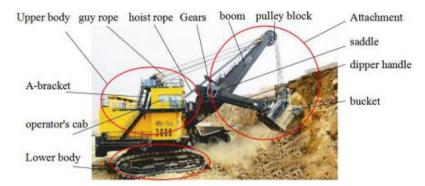
Fig. 1 The system composition of a typical large-scale excavator

Table 1 Main parameters of the excavator

Technical parameters of the excavator			
Total weight (*ton*)	1460	Theoretical yield (m^3/h)	6600
Hoisting speed (*m/s*)	1.58	Main motor powers (*KW*)	21000
Thrusting speed (*m/s*)	0.75	Maximum digging radius (*m*)	23.85
Hoisting force (*N*)	2890	Maximum digging height (*m*)	18.10
Thrusting force (*N*)	2227	Maximum permissible gradient (°)	13

2.2. The Kinematic Principle of Excavator Attachment

For an excavator, the excavator attachment is one of the most important factors influencing its performance. Therefore, the establishment of the kinematic sketch of excavator attachment is quite necessary before the dynamics simulation. The mathematical model of the attachment is shown in Fig. 2.

It can be seen from the Fig. 2 that $\angle DFE$ is the angle between the hoist rope and the center line of the dipper handle. It directly affects the magnitude of this force, which is along the dipper handle. As a result of the lifting force and the pushing force in the opposite direction, the pushing force will decrease and reduce power. Thus, in order to reduce the loss of energy, the angle of $\angle DFE$ could be increased as much as possible.

According to Fig. 2, the angle of $\angle DFE$ can be divided into two components:

$$\angle DFE = \theta_1 + \theta_2 \tag{1}$$

where $\angle DFE$ is the angle between the hoist rope and the dipper handle center line. θ_1 is the angle between the end of hoist rope to the center of pulley and the center line of the dipper handle. θ_2 is the angle between the end of the hoist rope to the center of pulley and the hoist rope. Furthermore:

$$O_2F = \sqrt{O_2C^2 + FC^2} \tag{2}$$

$$\angle DFE = \arccos \frac{O_1F^2 + O_2F^2 - O_1O_2^2}{2 \cdot O_1F \cdot O_2F} \tag{3}$$

where O_1F is the distance from the end of the hoist rope to the center of pulley. O_2F is the distance from the center of gear to the end of the hoist rope. O_1O_2 is the distance from the

center of the gear to the center of the pulley. O_2C is the equivalent distance to DF, which is the perpendicular distance from the center of the dipper handle (F) to O_1O_2. FC is the distance from the end of the hoist rope to O_2C.
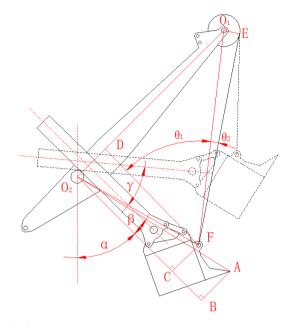

Fig. 2 The kinematic sketch of the excavator attachment

The bucket trajectory can be decomposed along the vertical and horizontal direction; the equations are given as:

$$\begin{cases} X = O_2A \cdot \sin(\alpha + \beta + \gamma) \\ Y = H - O_2A \cdot \cos(\alpha + \beta + \gamma) \end{cases} \tag{4}$$

where α is the angle between O_2C and the vertical direction. β is the angle between O_2C and the center line of the dipper handle. γ is the rotation angle of the dipper handle. H is the distance from the center of the gear to the ground.

The distance is defined in Eq. (5), which is from the pulley to the end of the hoist rope.

$$EF = \frac{O_1E}{\tan\theta_2} \tag{5}$$

where, O_1E is the distance from the center of the pulley to the center of the hoist rope.

2.3. The Differential Equations of Excavator Attachment

The dynamics of mechanical systems is usually described by high order differential equations. However, many parameters are involved in this higher-order differential equation. Therefore, in order to obtain an explicit expression between the parameters and

the system dynamic performance, the system dynamics model is often simplified.

The establishment of system differential equations needs to calculate the kinetic energy, potential energy and generalized force of the system. The kinetic energy of the lifting mechanism is given as:

$$T_1 = 2\left(\frac{1}{2}J_0\dot{\theta}_3^2 + \frac{1}{2}J_1\dot{\theta}_4^2 + \frac{1}{2}J_2i_1^2\dot{\theta}_4^2\right) + \frac{1}{2}J_3\dot{\theta}_5^2 + \frac{1}{2}J_4\dot{\theta}_5^2 + \frac{1}{2}m_1(\dot{\theta}_6l_1)^2 \tag{6}$$

where $J_i\,(i = 1,2, \ldots 4)$ are: the moment of inertia of the lifting motor, the driving gears of the lifting reducer, the driven gears of the lifting reducer and the roller, respectively; i is the transmission ratio of the gear; $\theta_i\ (i = 3,4,5)$ are the rotation angle of the lifting motor, the driving gears of the lifting reducer and the roller, respectively; θ_6 is the rotation angle between the boom and the platform; m_1 is the mass of the pulley; l_1 is the distance between the pulley and the hinge of the boom.

The kinetic energy of the dipper handle components is given as:

$$T_2 = \frac{1}{2}J_5\dot{\theta}_7^2 + \frac{1}{2}J_6\dot{\theta}_8^2 + J_7\dot{\theta}_9^2 + \left[\frac{1}{2}m_2(\dot{\theta}_6l_2)^2 + \frac{1}{2}m_3(\dot{\theta}_6l_3)^2 + \frac{1}{2}m_4(\dot{\theta}_6l_4)^2\right] \tag{7}$$

where $J_i\,(i = 5,6,7)$ is the moment of inertia of the crowd motor, the driving gears of the pushing reducer and the driven gears of the pushing reducer, respectively; $\theta_i\ (i = 7,8,9)$ are the rotation angles of the crowd motor, the driven gears of the lifting reducer and the crowd gear, respectively; $m_i\ (i = 2,3,4)$ are the mass of the pushing motor, driving gears and driven gears; l_2 is the distance between the pushing motor and the hinge of the boom; l_3 is the distance between the center of the belt and the hinge of the boom; l_4 is the distance between the pushing gear and the hinge of the boom. The kinetic energy of the execution components is given as:

$$T_3 = \frac{1}{2}J_8\dot{\theta}_6^2 + \frac{1}{2}(J_b + J_d)\dot{\theta}_{10}^2 + \frac{1}{2}(m_b + m_d)(\dot{S}_1 + 2\dot{S}_1\dot{S}_0 \cdot \sin\alpha_1 + \dot{S}_0^2) \tag{8}$$

where J_8, J_b and J_d are the moment of inertia of the boom, the dipper handle and the dipper, respectively; θ_{10} is the rotation angle of the dipper handle; m_b and m_d are the mass of the dipper handle and the dipper, respectively; α_1 angle between the hoist rope and the boom; S_0 is the dipper handle with the displacement of the boom; S_1 is the pushing gear with the displacement of the pushing motor. The total kinetic energy is given as:

$$\begin{aligned}
T &= T_1 + T_2 + T_3 \\
&= 2\left(\frac{1}{2}J_0\dot{\theta}_3^2 + \frac{1}{2}J_1\dot{\theta}_4^2 + \frac{1}{2}J_2i_1^2\dot{\theta}_4^2\right) + \frac{1}{2}J_3\dot{\theta}_5^2 + \frac{1}{2}J_4\dot{\theta}_5^2 + \frac{1}{2}m_1(\dot{\theta}_6l_1)^2 \\
&\quad + \frac{1}{2}J_5\dot{\theta}_7^2 + \frac{1}{2}J_6\dot{\theta}_8^2 + J_7\dot{\theta}_9^2 + \left[\frac{1}{2}m_2(\dot{\theta}_7l_2)^2 + \frac{1}{2}m_3(\dot{\theta}_7l_3)^2 + \frac{1}{2}m_4(\dot{\theta}_7l_4)^2\right] \\
&\quad + \frac{1}{2}J_8\dot{\theta}_6^2 + \frac{1}{2}(J_b + J_d)\dot{\theta}_{10}^2 + \frac{1}{2}(m_b + m_d)(\dot{S}_1 + 2\dot{S}_1\dot{S}_0 \cdot \sin\alpha_1 + \dot{S}_0^2)
\end{aligned} \tag{9}$$

Potential energy has many components, including the potential of the hoist rope components, the dipper handle and the boom. It is given as:

$$V_1 = \frac{1}{2}\frac{E_1 A_1}{l_5}\left(\frac{l_5 f_1}{E_1 A_1} + R\boldsymbol{\theta}_2 + O_2 C \cdot \boldsymbol{\theta}_{10}\sin\boldsymbol{\theta}_1 - l_1\boldsymbol{\theta}_6\sin\alpha_1\right)^2 + k_1(\boldsymbol{\theta}_4 - \boldsymbol{\theta}_3)^2 + \frac{1}{2}k_2\left(\boldsymbol{\theta}_5 - \frac{\boldsymbol{\theta}_4}{i_1}\right)^2 \quad (10)$$

where A_1 is the sum of cross-sectional areas of the hoist rope; l_5 is the length of deformation of the hoist rope; f_1 is the hoist rope lifting force; k_i ($i = 1,2$) is torsional rigidity of the lifting motor and roller, respectively; E_1 is the elastic modulus of the hoist rope; R is the diameter of the drum.

The potential energy of the dipper handle is given by:

$$V_2 = \frac{1}{2}\frac{E_2 A_2}{DF}\left(\frac{F \cdot DF}{E_3 A_3} + r\boldsymbol{\theta}_9 + l_7\boldsymbol{\theta}_6\cos\left(\alpha_1 - \frac{\pi}{2}\right)\right)^2 + \frac{1}{2}\left(\frac{E_1 A_1}{l_9}R\boldsymbol{\theta}_5\right)^2\sin^2\phi\frac{b^2 \cdot O_2 C^3}{3E_3 I \cdot O_2 A^2}$$
$$+ \frac{1}{2}k_3(\boldsymbol{\theta}_7 R_1 - \boldsymbol{\theta}_6 R_2)^2 + \frac{1}{2}k_4(\boldsymbol{\theta}_8 - \boldsymbol{\theta}_7)^2 \qquad (11)$$

where A_i ($i = 2,3$) is cross-sectional areas of the guy rope and the dipper handle, respectively; E_i ($i = 2,3$) is elastic modulus of the guy rope and the dipper handle, respectively; k_i ($i = 4,5$) is torsional rigidity of the belt and between the belt and the belt pulley, respectively; R_i ($i = 1,2$) is the diameter of the driving belt pulley and the driven belt pulley, respectively; F is thrust of the dipper handle; r is radius of the gear for the dipper handle; l_6 is total length of the hoist rope; l_7 is the width of the boom connection; I is the moment of inertia of the dipper handle. The potential energy of the boom is given as:

$$V_3 = \frac{(f_1' + f_2')^2 l_1}{2E_4 A_4} \qquad (12)$$

where f_1' is the hoist rope force acting on the boom; f_2' is the guy rope force acting on the boom; A_4 is cross-sectional areas of the boom; E_4 is elastic modulus of the boom. The total potential energy is given as:

$$V = V_1 + V_2 + V_3$$
$$= \frac{1}{2}\frac{E_1 A_1}{l_5}\left(\frac{l_5 f_1}{E_1 A_1} + R\boldsymbol{\theta}_5 + O_2 C \cdot \boldsymbol{\theta}_{10}\sin\boldsymbol{\theta}_1 - l_1\boldsymbol{\theta}_6\sin\alpha_1\right)^2 + k_1(\boldsymbol{\theta}_4 - \boldsymbol{\theta}_3)^2 + \frac{1}{2}k_2\left(\boldsymbol{\theta}_5 - \frac{\boldsymbol{\theta}_4}{i_1}\right)^2$$
$$+ \frac{1}{2}\frac{E_2 A_2}{DF}\left(\frac{F \cdot DF}{E_3 A_3} + r\boldsymbol{\theta}_9 + l_7\boldsymbol{\theta}_6\cos\left(\alpha_1 - \frac{\pi}{2}\right)\right)^2 + \frac{1}{2}k_3(\boldsymbol{\theta}_7 R_1 - \boldsymbol{\theta}_6 R_2)^2 + \frac{1}{2}k_4(\boldsymbol{\theta}_8 - \boldsymbol{\theta}_7)^2 \qquad (13)$$
$$+ \frac{1}{2}\left(\frac{E_1 A_1}{l_9}R\boldsymbol{\theta}_5\right)^2\sin^2\phi\frac{b^2 \cdot O_2 C^3}{3E_3 I \cdot O_2 A^2} + \frac{(f_1' + f_2')^2 l_1}{2E_4 A_4}$$

According to the Lagrange generalized coordinates, the equation of motion can be given as:

$$\frac{d}{dt}\left(\frac{\partial T}{\partial \dot{q}_i}\right) - \frac{\partial T}{\partial q_i} + \frac{\partial V}{\partial q_i} + \frac{\partial D}{\partial \dot{q}_i} = Q_i \quad (i = 1, 2, \cdots n) \qquad (14)$$

By substituting Eqs. (12) and (13) into Eq. (14), the differential equation of motion reads:

$$
\begin{cases}
2J_0\ddot{\theta}_3 + 2k_1(\theta_4 - \theta_3) = 2Q_s \\[2mm]
2J_1\ddot{\theta}_4 + 2J_{21}^2\ddot{\theta}_4 + 2k_1(\theta_4 - \theta_3) + k_2\left(\theta_5 - \dfrac{\theta_4}{i_1}\right) = 0 \\[2mm]
J_3\ddot{\theta}_5 + J_4\ddot{\theta}_5 + k_2\left(\theta_5 - \dfrac{\theta_4}{i_1}\right) + \left(\dfrac{E_1A_1}{l_9}\right)^2 R^2\theta_5\sin^2\phi\,\dfrac{b^2 \cdot O_2C^3}{3E_3I \cdot O_2A^2} = 0 \\[2mm]
m_1l_1^2\ddot{\theta}_6 + J_8\ddot{\theta}_6 + \dfrac{E_1A_1}{l_5}\left(\dfrac{l_5f_1}{E_1A_1} + R\theta_5 + O_2C \cdot \theta_{10}\sin\theta_1 - l_1\theta_6\sin\alpha_1\right)l_1\sin\alpha_1 \\[2mm]
\quad + \dfrac{E_2A_2}{DF}\left(\dfrac{F \cdot DF}{E_3A_3} + r\theta_9 + l_7\theta_6\cos\left(\alpha_1 - \dfrac{\pi}{2}\right)\right)l_7\cos\left(\alpha_1 - \dfrac{\pi}{2}\right) = Q_t \\[2mm]
J_5\ddot{\theta}_7 + m_2(\ddot{\theta}_7l_2)l_2 + m_3(\ddot{\theta}_7l_3)l_3 + m_4(\ddot{\theta}_7l_4)l_4 + k_3R_1(\theta_7R_1 - \theta_6R_2) + k_4(\theta_8 - \theta_7) = 0 \\[2mm]
J_6\ddot{\theta}_8 + k_4(\theta_8 - \theta_7) = 0 \\[2mm]
2J_7\ddot{\theta}_9 + \dfrac{E_2A_2}{DF}r\left(\dfrac{F \cdot DF}{E_3A_3} + r\theta_9 + l_7\theta_6\cos\left(\alpha_1 - \dfrac{\pi}{2}\right)\right) = 0 \\[2mm]
(J_b + J_d)\ddot{\theta}_{10} + \dfrac{E_1A_1}{l_5}\left(\dfrac{l_5f_1}{E_1A_1} + R\theta_5 + O_2C \cdot \theta_{10}\sin\theta_1 - l_1\theta_6\sin\alpha_1\right)O_2C \cdot \sin\theta_1 = 0
\end{cases}
\tag{15}
$$

where Q_s is the torque of the lifting motor; Q_t is the torque of the crowd motor.

3. SETTING UP THE DYNAMIC MODEL

The objective of this paper is to obtain the dynamics performance of the excavator attachment during one digging process. Therefore, the lower body and its associated effect have been ignored in the current work. The 3D dynamic model is established and imported into ADAMS.

As the boom and the dipper handle make a great effect on the excavator, it is better to define them as flexible bodies in the simulation, which will generate more realistic results compared with the conventional full rigid simulation.

3.1. Grid-Independent Descriptors

In order to obtain an accurate model and reduce computing time, a grid independent analysis has been carried out. This work compares the first order natural frequency of the boom and the dipper handle with different grids.

As shown in Figs. 3 and 4, the frequency tends to be stable as the number of grids increases. It can be found that the frequency is independent of the number of grids when the number of grids is greater than 2.8×10^6. This paper proposes a method for the components which allow for local grid refinement. The rigid regions of the boom and the dipper handle

are set in accordance with the actual situation. It can not only guarantee the accuracy of the results, but it can also reduce the computing time.
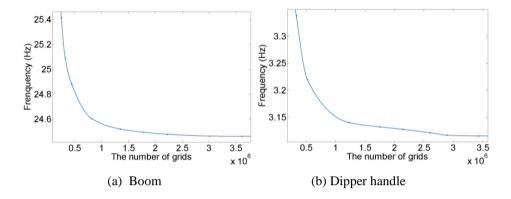

(a) Boom   (b) Dipper handle

Fig. 3 The kinematic sketch of the excavator attachment

3.2. Modal Calculation

The flexible body model has been established in the ANSYS environment, as described in Section 3, which can be used for calculating its eigenfrequencies and its eigenmodes [18,19]. The eigenfrequencies and eigenmodes are analyzed theoretically in this study. In order to resolve these important dynamic parameters of the system, the free vibration equation of the system is obtained by ignoring the damping factors in the system:

$$[\mathbf{M}]\{\ddot{y}\} + [\mathbf{K}]\{y\} = \{\mathbf{0}\} \tag{16}$$

where $\mathbf{M}$ and $\mathbf{K}$ are the mass matrix and stiffness matrices of the component, respectively, y are displacements.

Suppose the differential Eq. (1) has the following form of results:

$$\{y\} = \{\mathbf{u}\}\sin(\boldsymbol{\phi}_1 t + \boldsymbol{\lambda}) \tag{17}$$

where $\{\mathbf{u}\}$ is the eigenmode vector; $\boldsymbol{\phi}_1$ is the frequency of simple harmonic motion; $\boldsymbol{\lambda}$ is the initial phase angle. $\{\mathbf{u}\}$ is given as:

$$\{\mathbf{u}\} = \{u_1 \quad u_2 \quad u_3 \cdots u_n\}^T \tag{18}$$

By substituting Eq. (17) into Eq. (16), a new equation is obtained:

$$\left([\mathbf{K}] - \boldsymbol{\phi}_1^2 [\mathbf{M}]\right)\{\mathbf{u}\} = \{\mathbf{0}\} \tag{19}$$

The eigenfrequencies and the eigenmodes are then defined by the following equation:

$$[\mathbf{M}]^{-1}[\mathbf{K}]\{\mathbf{u}\} = \boldsymbol{\phi}^2 \{\mathbf{u}\} \tag{20}$$

Figs. 4 and 5 depict the eigenfrequencies and eigenmodes of the boom and the dipper handle. In order to avoid resonance and improve the excavator performance, the researchers modify the structure of the boom and the dipper handle, which can achieve the objective.
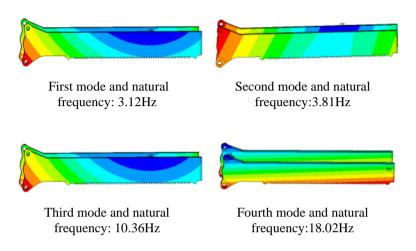
First mode and natural
frequency: 3.12Hz

Second mode and natural
frequency:3.81Hz

Third mode and natural
frequency: 10.36Hz

Fourth mode and natural
frequency:18.02Hz

Fig. 4 Dipper handle: eigenfrequencies and eigenmodes computation

First mode and natural
frequency: 24.52Hz

Second mode and natural
frequency: 28.50Hz

Third mode and natural
frequency: 32.87Hz

Fourth mode and natural
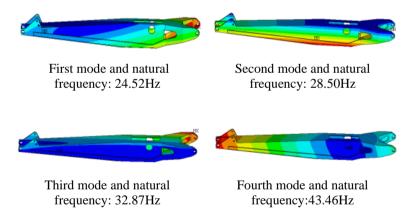frequency:43.46Hz

Fig. 5 Boom: eigenfrequencies and eigenmodes computation

The boom and the dipper handle used in this case have the same general characteristics as those studied previously, except that the boom and the dipper handle are now taken as a flexible body. The boom and the dipper handle are saved as the neutral file (.mnf) and imported into the ADAMS to obtain a rigid-flexible coupling model of the attachment. The rigid-flexible coupling model is shown in Fig. 6.
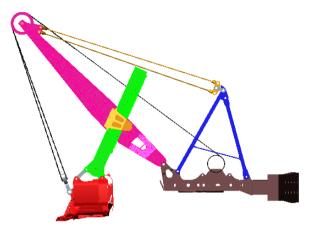
Fig. 6 Rigid-flexible coupled model

4. NUMERICAL SIMULATION SETTINGS

4.1. Basic Assumptions of the Model

The kinematics principle of excavators is extremely complex and the main reason for this is that vibration exists in the process; it is very important to simplify the model and give the basic assumptions. Therefore, this paper makes following basic assumptions:

(i) This paper will not consider the dimension tolerance of the model and various errors;

(ii) In addition to the boom, the dipper handle and the hoist rope, the other parts of the system are treated as rigid bodies.

The initial condition of the rigid-flexible model is shown in Table 2.

Table 2 The initial conditions of the excavator

Components	Position
Boom	The boom is fixed;
Dipper handle	The distance is 12.1 m, which is between the gear shaft and the ground. The angle is 23.8°, which is between the axis of the dipper handle and the vertical direction.

4.2. Constraints and Motions

In order to ensure the reliability of the excavator model, the constraints are set according to the actual situation, which are shown in Table 3.

Table 3 The constraints of the excavator

	Boom	Dipper handle	Pulley	Bucket	Saddle	Guy rope	Hoist rope	Platform
Boom	—	—	R	—	R	R	—	R
Dipper handle	—	—	R	R	C	—	—	—
Pulley	R	R	—	R	—	—	C	—
Bucket	—	R	R	—	—	—	R	—
Saddle	R	C	—	—	—	—	—	—
Guy rope	R	—	—	—	—	—	—	—
Hoist rope	—	—	C	R	—	—	—	R
Platform	R	—	—	—	—	—	R	—

where R represents rotation; C represents contact.

To give the resistance force applied to the bucket, EDEM is used to simulate one digging cycle; Figs. 7-9 show the mass change, the resistance force change, and the control velocities of the dipper handle and the hoist rope, respectively.
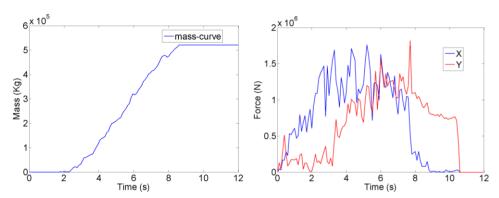

Fig. 7 Mass change during the mining process **Fig. 8** Resistance force change during the process
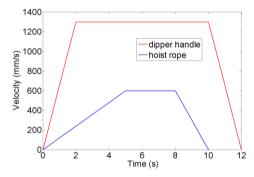

Fig. 9 Control velocity of the hoist rope and dipper handle

4.3. Solver Setting

ADAMS/Solver uses multistep integration methods that contain a predictor and a corrector [20,21]. ADAMS has many integrators and formulations to meet different requirements.

In this paper, the researcher chooses the Gear Stiff integrator (GSTIFF) and the integrator formulation (SI1), which takes into account the constraint derivatives when solving the equations of motion just as it monitors the integration error on the impulse of the Lagrange Multipliers in the system [21]. This work selects the integration tolerance as 0.001, the simulation time is 12s and the step size is 0.02s.

5. RESULTS

In order to catch the dynamic characteristics of the excavator, it can be divided into two cases in order to carry out a rigid-flexible coupling study. One case is that the dipper handle is regarded as a rigid body and the boom is regarded as a flexible body while the other case is that the dipper handle and the boom are both regarded as a flexible body. The trajectory of the excavator is shown in Fig. 10.
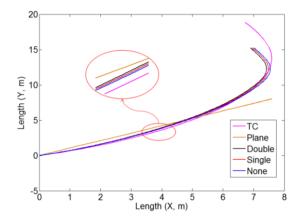

Fig. 10 Trajectory of the excavator

where TC is the theoretical curve trajectory; Plane is the plane before the material is excavated; Double, Single and None are the trajectory of different number of flexible bodies, respectively.

As shown in Fig.10, the value of the (TC) is significantly lower than the simulation value; the main reason is that there is vibration during the whole process. In conjunction with the results of the simulation, the number of the flexible body has little effect on the trajectory, and the rigid body is closer to the theoretical trajectory. The study concludes that the excavator in the process is not steady in work and that certain vibration exists.

In this study, the stress distribution is obtained according to the post-processing module. The top ten maximum stress nodes as well as their occurrence times are when the boom and the dipper handle are in the state of maximum stress. The results of the boom are shown in Figs. 11 and 12 and Table 4.

Fig. 11 illustrates that the maximum stress is located at node 294. The value of the stress is 212.24 MPa and it occurs at time 5.72 s. The node is located at the boom corner. This is the position exposed to a high risk of failure.

The objective is to obtain the stress curve which is 294th node in the entire process. Firstly, this study obtains the load spectrum from ADAMS and imports it into the ANSYS. Then, the load spectrum is loaded into the model, which calculates the modality information. The Von Mises stress curve of the 294th node can be obtained in the post-processing module of ANSYS. The stress mainly is concentrated in 70-175 MPa of the 294th node in the whole process. Hence, the boom meets the strength requirements.

Table 4 The maximum stress node number and position of the boom

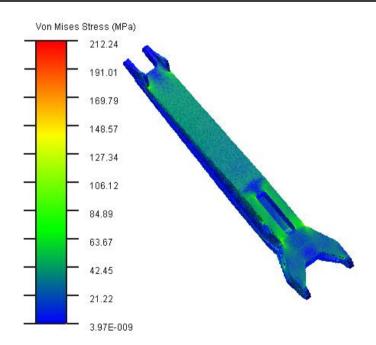| Hot Spot	Stress	Node	Time	Location (*mm*)		
#	*MPa*	*id*	(*sec*)	X	Y	Z
1	212.27	294	5.72	-2117.33	2418.46	6291.37
2	189.02	826	5.72	-1959.91	2307.07	4309.16
3	184.75	187077	6.39	-2135	2418.98	6291.37
4	192.43	146014	5.72	-2424.58	1972.99	4351.58
5	181.08	296	5.72	-2134.49	2436.64	6291.37
6	178.99	496	5.72	-2411.37	1976.95	4366.2
7	174.10	146015	5.72	-2425.18	1972.71	4338.11
8	173.53	19612	5.72	-3616.54	1037.46	4391.37
9	172.55	58	5.72	-2415.69	1976.09	4325.26
10	169.48	29260	5.72	-2135.51	2401.3	6291.37

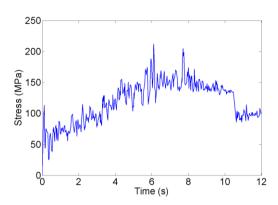**Fig. 11** Stress distribution of the boom

Fig. 12 The stress curve of node 294

The dipper handle is a core component of the attachment. The results of the dipper handle are shown in Figs. 13 and 14 as well as Table 5.

From Fig. 13, it can be seen that the maximum stress is located at node 70. Its value is 96.45 MPa, and it occurs at time 3.27 s. The maximum stress occurs in the holes that enable connection with the bucket. This position is at the highest risk of failure.
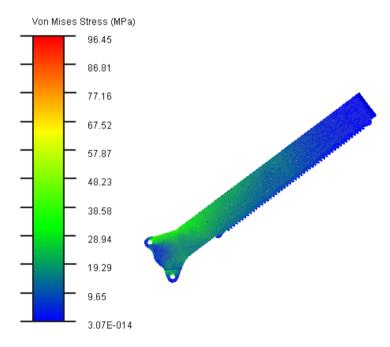
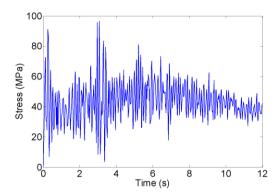

Fig. 13 Stress distribution of the dipper handle

Fig. 14 The stress curve of 70th node

Table 5 The maximum stress node number and position of the dipper handle

Hot Spot #	Stress MPa	Node id	Time (sec)	Location (mm)		
				X	Y	Z
1	96.45	70	3.27	-6906.14	-3265.95	3822.05
2	95.23	69	3.30	-6906.14	-3265.94	4115.05
3	92.53	3256	3.27	-6930.42	-3245.89	3822.05
4	86.71	3173	3.30	-6930.42	-3245.88	4115.05
5	83.41	49626	3.30	-6902.92	-3234.28	4115.05
6	82.02	49358	3.30	-6871.51	-3269.42	4146.55
7	79.75	49865	3.27	-6904.16	-3233.27	3822.05
8	78.90	2838	3.30	-6882.79	-3287.08	4146.55
9	78.10	2399	3.27	-6293.56	-2350.94	3746.04
10	77.51	39203	3.27	-6917.16	-3256.16	3805.85

The main reasons for this can be broadly classified into two types. One refers to the clearances between the dipper handle and the saddle while the other is the uneven distribution of the wire rope in the mining process. In order to investigate the influence of the clearances on the boom, this paper studies the clearances of 0-14 mm while the results are shown in Figs. 15-18.

Fig. 15 illustrates that the vibration of the boom is most noticeable in the Y direction, followed by the X direction and Z direction. For example, the amplitude vibration range of the boom is mainly between 6349 mm and 6357 mm in the Y direction. This paper has analyzed the clearance effect of different directions, and obtained the probability density distribution.

This study obtains the Von Mises stress curve of the dipper handle by using the same method as above. The stress mainly is concentrated in 20-60 MPa at node 70 in the whole process. Hence, the dipper handle meets the strength requirements. As shown by the above analysis, it can be clearly seen that it is easier for the boom to fail than for the dipper handle.
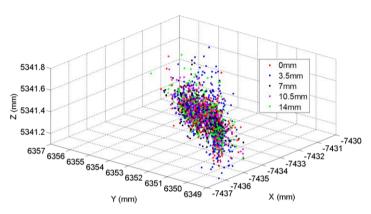
Fig. 15 The influence of different clearances on the boom in the 3D space
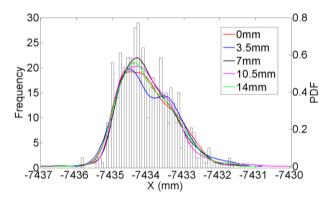

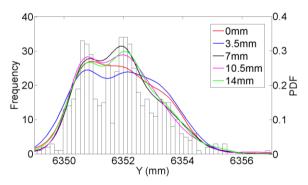**Fig. 16** The influence of different clearances on the boom in the X direction

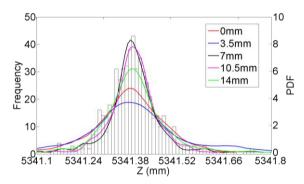**Fig. 17** The influence of different clearances on the boom in the Y direction

Fig. 18 The influences of different clearances on the boom in the Z direction

It can be observed from Figs. 16-18 that the boom vibration is similar to the normal distribution in different directions. In the X direction, with the clearance decreasing, the vibratory magnitude of the boom decreases at first, and then increases. The Y direction and Z direction are similar to the X direction. The boom vibration is most noticeable in the Y direction and X direction; the optimal value is near 3.5 mm. The variances of the different clearances are shown in Table 6.

Table 6 The variance of the different clearances in different directions

	X	Y	Z
0mm	0.71	1.28	0.11
3.5mm	0.69	1.22	0.07
7mm	0.77	1.32	0.16
10.5mm	0.72	1.26	0.06
14mm	0.72	1.25	0.08

In order to investigate the influence of clearances on the dipper handle, this study examines the clearances of 0-14 mm; the results are shown in Figs. 19-22.
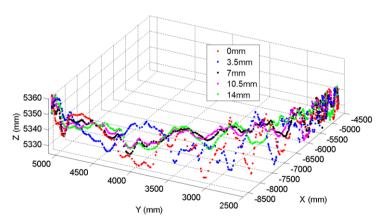

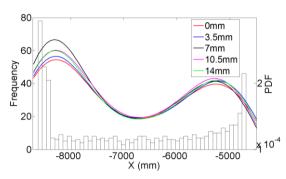**Fig. 19** The influences of different clearances on the dipper handle in the 3D space

Fig. 20 The influences of different clearances on the dipper handle in the X direction
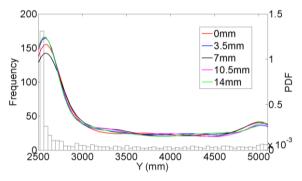

Fig. 21 The influences of different clearances on the dipper handle in the Y direction
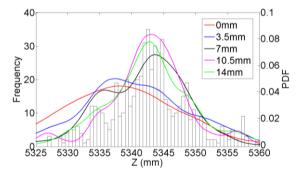

Fig. 22 The influences of different clearances on the dipper handle in the Z direction

Fig. 19 illustrates that the range of motion is relatively large in the 3D space. The main reason for this is that the dipper handle is moving. The clearance effects of different directions are analyzed in this paper and the probability density distribution is obtained. Figs. 22-25 illustrate the influences of different clearances on the dipper handle in different directions. Obviously, the effect in the Z direction is smaller than in the X direction and Y direction. The vibration amplitude of the dipper handle is the smallest when the clearance value is 3.5 mm. Therefore, it can be concluded that the optimal value is near 3.5 mm. In addition, the variances of the different clearances in different directions are shown in Table 7.

Table 7 The variance of the different clearances in different directions

	X	Y	Z
0mm	1446.32	930.54	5.96
3.5mm	1449.42	904.89	5.87
7mm	1484.51	925.97	8.48
10.5mm	1480.90	908.08	8.24
14mm	1469.57	925.63	6.18

In order to study the influence of the clearances on the lifting force, this study examines the clearances of 0-14 mm and the results are shown in Fig. 23.
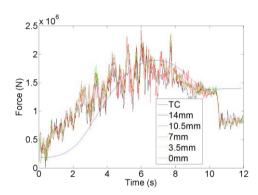

Fig. 23 The influences of different clearances on the force of the hoisting ropes

Fig. 23 shows that the value of the theoretical curve (TC) is significantly lower than the simulation value. The main reason is that the dipper handle as well as the bucket has the vibration in the whole process. When the clearance value is 3.5 mm, the force of the hoisting ropes is the smallest. The deviation is about 25% between the simulation and the theoretical value in the acceleration phase. In the stationary phase, the deviation value is about 5.6%. When the bucket is out of the material, the value of simulation is lower than the value of TC, mainly resulting from the fact that friction becomes ineffective.

6. CONCLUSION

Dynamic performance of the intelligent excavating process is developed in this paper. Firstly, the structure and primary performance parameters are introduced. Then, the rigid-flexible coupling virtual prototyping model of the excavator attachment is established. In addition, the stress distribution is obtained, including the top ten maximum stress nodes and the stress curves. To explore the laws of the influence of flexible body and clearance, the comparisons between different excavating scenarios with respect to different clearances are conducted. The results show that with the clearance decreasing, the vibratory magnitude of the boom decreases firstly, and then increases. The actual model with different clearances of macroscopic fluctuations is taken into account in the numerical experiments for the analysis of the excavator's dynamic characteristic. It can be seen that the analysis of the dynamic characteristic model is flexible and available.

The excavator is complex equipment, which consists of three major components, including the upper body, the lower body and the attachment. All the corresponding structures exert great influences on the dynamic performance. For the future work, it is planned that the dynamic performance will be also taken into account and dealt with the structure parameters of the boom and the dipper handle.

REFERENCES

1. Li, Y., Liu, W., 2013, *Dynamic dragline modeling for operation performance simulation and fatigue life prediction*，Engineering Failure Analysis, 34, pp. 93-101.
2. Li, Y., Frimpong, S., 2008, *Hybrid virtual prototype for analyzing cable shovel component stress*, The International Journal of Advanced Manufacturing Technology, 37(5), pp. 423-430 .
3. Jovanović, V., Janošević, D., Pavlović, J., 2021, *Analysis of the influence of the digging position on the loading of the axial bearing of slewing platform drive mechanisms in hydraulic excavators*, Facta Universitatis-Series Mechanical Engineering, 19(4), pp. 705-718.
4. Mitrev, R., Marinković, D., 2019, *Numerical study of the hydraulic excavator overturning stability during performing lifting operations,* Advances in Mechanical Engineering, 11(5), doi: 10.1177/1687814019841779.
5. Li, Y., Chang, S.S., 2013, Liu, W., *Spatial kinematics and virtual prototype modeling of Bucyrus shovel*, International Journal of Advanced Manufacturing Technology, 69(5-8), pp. 1917-1925.
6. Awuah-Offei, K., Frimpong, S., 2007, *Cable shovel digging optimization for energy efficiency*, Mechanism and machine theory, 42(8), pp. 995-1006.
7. Šalinić, S., Bošković, G., Nikolić, M., 2014, *Dynamic modelling of hydraulic excavator motion using Kane's equations*, Automation in Construction, 44, pp. 56-62.
8. Awuah-Offei, K., Frimpong, S., 2006, *Numerical simulation of cable shovel resistive forces in oil sands excavation*, International Journal of Surface Mining, Reclamation and Environment, 20(3), pp. 223-238.
9. Mitrev, R., Janošević, D., Marinković, D., 2017, *Dynamical modelling of hydraulic excavator considered as a multibody system*, Tehnicki Vjesnik, 24, pp. 327-338.
10. Ding, H, Han, L, Yang, W, et al., 2017, *Kinematics and dynamics analyses of a new type face-shovel hydraulic excavator*, Proceedings of the Institution of Mechanical Engineers, Part C: Journal of Mechanical Engineering Science, 231(5): 909-924.
11. Ma, M.H, 2009, *Research on dynamic characteristics of working equipment of mining excavator*, Master Thesis, Jilin University.
12. He, B., Zhou, G.F., Hou, S. C., Zeng, L., 2017, *Virtual prototyping-based fatigue analysis and simulation of crankshaft*, The International Journal of Advanced Manufacturing Technology, 88(9-12), pp. 2631-2650.
13. He, B., Tang, W., Cao, J.T., 2014, *Virtual prototyping-based multibody systems dynamics analysis of offshore crane*, The International Journal of Advanced Manufacturing Technology, 75(1-4), pp. 161-180
14. Jiang, M., Liao, S., Guo, Y., Wu, J., 2019, *The improvement on vibration isolation performance of hydraulic excavators based on the optimization of powertrain mounting system*, Advances in Mechanical Engineering, 11(5), doi: 10.1177/1687814019849988.
15. Strzalka, C., Marinkovic, D., Zehn, M.W., 2021, *Stress mode superposition for a priori detection of highly stressed areas: mode normalisation and loading influence*, Journal of Applied and Computational Mechanics, 7(3), pp. 1698-1709.
16. Strzalka, C., Zehn, M., 2020, *The influence of loading position in a priori high stress detection using mode superposition*, Reports in Mechanical Engineering, 1(1), pp. 93-102.
17. Zhao, H , Wang, G.Q., Wang, H.T., Bi, Q.S., Li, X.F., 2017, *Fatigue life analysis of crawler chain link of the excavator*, Engineering Failure Analysis, 79, pp. 737-748.
18. Zhang, Y.Z., Wang, Y.T., 2008, *Co-simulation of Flexible Body Based on ANSYS and ADAMS*, Journal of system simulation, 20, pp. 4501-4504.

19. Khemili, I., Romdhane, L., 2008, *Dynamic analysis of a flexible slider-crank mechanism with clearance*, European Journal of Mechanics-A/Solids, 27(5), pp. 882-898.
20. Yuan, Y.L., Yang, Z., Wang, S.H., Li, X.F., 2014, *The Application and Analysis of Gear Train in the Turnover Mechanism*, Packaging Engineering, 17(9), pp. 86-90.
21. Chen, Y., Sun, Y., Chen, C., 2016, *Dynamic analysis of a planar slider-crank mechanism with clearance for a high speed and heavy load press system*, Mechanism and Machine Theory, 98, pp. 81-100.